Chemical Science

RSC Publishing

EDGE ARTICLE

View Article Online
View Journal | View Issue

Cite this: *Chem. Sci.*, 2013, **4**, 2912

A theoretical and experimental examination of systematic ligand-induced disorder in Au dendrimer-encapsulated nanoparticles†

David F. Yancey,[ab] Samuel T. Chill,[ac] Liang Zhang,[ac] Anatoly I. Frenkel,*[d] Graeme Henkelman*[ac] and Richard M. Crooks*[ab]

Received 5th March 2013
Accepted 30th April 2013

DOI: 10.1039/c3sc50614b

www.rsc.org/chemicalscience

In this paper we present a new methodology for the analysis of 1–2 nm nanoparticles using extended X-ray absorption fine structure (EXAFS) spectroscopy. Different numbers of thiols were introduced onto the surfaces of dendrimer-encapsulated Au nanoparticles, consisting of an average of 147 atoms, to systematically tune the nanoparticle disorder. An analogous system was investigated using density functional theory molecular dynamics (DFT-MD) simulations to produce theoretical EXAFS signals that could be directly compared to the experimental results. Validation of the theoretical results by comparing to experiment allows us to infer previously unknown details of structure and dynamics of the nanoparticles. Additionally, the structural information that is learned from theoretical studies can be compared with traditional EXAFS fitting results to identify and rationalize any errors in the experimental fit. This study demonstrates that DFT-MD simulations accurately depict complex experimental systems in which we have control over nanoparticle disorder, and shows the advantages of using a combined experimental/theoretical approach over standard EXAFS fitting methodologies for determining the structural parameters of metallic nanoparticles.

Introduction

Accurate characterization of nanoparticle catalysts and electrocatalysts is crucial for understanding the fundamental relationship between their structure and catalytic function, and the key requirement for achieving this goal is the development of more sophisticated structural tools and methods.[1–3] One analytical method that is particularly amenable to combined theoretical and experimental studies is extended X-ray absorption fine structure (EXAFS) spectroscopy, and particularly its application to the analysis of small metallic nanoparticles. In this case, the interplay of theory and experiment provides a means to extract more accurate structural information from experimental EXAFS signals and to reduce the effects of fitting artifacts that arise in disordered systems.[1,3] For example, one important limitation of EXAFS analysis is that it provides averaged information about the structure and dynamics of the nearest environment of all absorbing atoms in the nanoparticle ensemble, and this can lead to erroneous structural determinations if an "average" configuration is assumed to be the actual configuration. Specifically, if the distribution of sizes, shapes, crystal structures, and states of order is broad,[4–6] then the notion of a "representative" nanoparticle is unhelpful at best, or, as recently shown, can lead to misinterpretation.[6]

Another challenge in the 3D refinement of EXAFS data of nanoparticle systems is the appropriateness of the assumption of small to moderate disorder, which refers to the time- and configuration-averaged profile of the metal–metal pair distribution function (PDF).[1,3] For quasi-Gaussian distributions, EXAFS is able to correctly account for disorder and produces accurate structural and dynamic characteristics (bond lengths and bond length disorders, also known as the Debye–Waller factors in EXAFS).[7] Unlike the symmetric bond length distributions that are typically observed in bulk materials, the distribution for nanoparticles is expected to be asymmetric since the bond lengths at the surface deviate from those in the core of the particle.

Approaches that correctly address this problem have recently appeared in the literature.[1,2,8] These approaches are based on calculating EXAFS spectral contribution from each atom in the cluster, and then performing temporal averaging of the results. As this and other approaches continue to evolve, the need for a good experimental model against which to judge theoretical

[a]*Department of Chemistry and Biochemistry, 105 E 24th St. Stop A5300, Austin, TX 78712-0165, USA. E-mail: crooks@cm.utexas.edu; henkelman@cm.utexas.edu; Tel: +1 512-475-8674; +1 512-471-4179*

[b]*Texas Materials Institute, 105 E 24th St. Stop A5300, Austin, TX 78712-0165, USA*

[c]*Institute for Computational and Engineering Sciences, The University of Texas at Austin Department of Chemistry and Biochemistry, 105 E 24th St. Stop A5300, Austin, TX 78712-0165, USA*

[d]*Physics Department, Yeshiva University, 245 Lexington Avenue, New York, NY 10016, USA. E-mail: anatoly.frenkel@yu.edu; Tel: +1 212-340-7827*

† Electronic supplementary information (ESI) available. See DOI: 10.1039/c3sc50614b

treatments has become critical. This is exactly the objective of the present report. We are describing a stable, well-defined, monodisperse, and relatively simple (compared to supported nanoparticles) model system with tunable structural disorder.

The experimental model is Au dendrimer-encapsulated nanoparticles (DENs) containing an average of 147 atoms per particle (Au_{147}).[9] DENs are synthesized in two steps. First, metal salts are introduced to the interior of the dendrimer structure. Second, the resulting composite is chemically reduced to yield a nanoparticle encapsulated within the dendrimer template. Because the synthesis is kinetically controlled, DENs exhibit remarkable size and structural monodispersity. For the purposes of the present report, there are two properties of DENs that are important. First, DENs are unsupported nanoparticles, and therefore any influence exerted on particle structure by a surface is obviated. This is important, because it is difficult to separate the effects of strong metal–support interactions and metal–ligand interactions on nanoparticle structure.[10–13] Second, DENs are sterically trapped within the dendrimers, and the Au surface does not interact strongly with the dendrimer host.[9] One consequence of this is that the Au surface is accessible to small molecules. For example, we have previously shown that thiols easily penetrate the dendrimer and adsorb strongly to the surface of the encapsulated nanoparticle.[14,15] Here, we take advantage of this observation by using different surface concentrations of thiols to modulate the structural disorder of the DENs.

In this report, we compare experimental EXAFS results with theoretically generated EXAFS data from analogous nanoparticles using density functional theory molecular dynamics (DFT-MD) simulations. Achieving good agreement between the experimental and theoretical EXAFS signals provides two advantages over conventional EXAFS analysis. First, it validates the theoretical method used as accurately describing the experimental system. From this, we can obtain otherwise unknown structural and dynamical properties of the nanoparticle systems directly from theory. Second, structural properties learned from theoretical simulations can be directly compared with those obtained by conventional EXAFS analysis in which structure and dynamics are obtained in terms of the coordination numbers, bond lengths, and disorder parameters. If the structural properties obtained from theory differ from parameters extracted from traditional EXAFS fitting of experimental data, we can begin to rationalize where standard EXAFS fitting breaks down and how to develop corrective measures.

One of the most common synthetic methods for preparing monodisperse Au nanoparticles involves quenching their growth and stabilizing their size with functionalized thiols.[16–22] A recent and important advance in our understanding of the structural properties of thiol-capped Au nanoparticles resulted from crystallization and X-ray crystallographic analysis of small (25–38 atoms) Au nanoclusters.[23–26] These studies showed that in the presence of thiol ligands some surface Au atoms exist in staple motifs, in which these atoms are displaced from the Au surface. These thiol-capped nanoparticles are also influenced by inter-ligand interactions. Importantly, however, the thiol-capping synthetic method results in nanoparticles having surfaces that are fully saturated with ligands, and therefore it is not possible to use this approach for examining the structure of the Au core as a function of the surface ligand density. In contrast, the approach described here provides a convenient method for controlling the surface ligand density. Moreover, the specific ligand we have chosen, 2-mercaptoethanol, is sufficiently short that inter-ligand interactions are minimized.[27] Consequently, the present study provides insight into how the structure of Au nanoparticles is affected by different surface concentrations of thiol ligands.

The key aspect of this work is that we have validated DFT-MD simulations of Au_{147} DENs having varying amounts of thiols bound to the surface by comparing theoretical and experimental EXAFS spectra on exactly analogous particles. To accomplish this goal, we developed an experimental approach for modulating the disorder of Au_{147} DENs by controlling the surface ligand density. EXAFS fitting reveals that a slight bond length expansion and an increase in Au–Au bond disorder correlate with increasing thiol surface concentration. The theory-based EXAFS modeling strategy was used to generate theoretical EXAFS spectra, which were then fit with the same approach used for the experimental results. Interestingly, the average bond length and disorder values calculated directly from the MD trajectories are in poor agreement with results extracted from EXAFS analysis of the same data. However, standard EXAFS fitting gives similar results for both experimental and theoretical EXAFS signals in terms of coordination numbers, average bond lengths, and Debye–Waller factors.

Experimental section

Chemicals

Amine-terminated, sixth-generation poly(amidoamine) (PAMAM) dendrimers (G6-NH_2) in methanol were purchased from Dendritech, Inc. (Midland, MI). The methanol was evaporated under vacuum and the dendrimer was reconstituted in H_2O at a concentration of 100 μM. The following chemicals were purchased from Sigma-Aldrich and used as received: $HAuCl_4$, $NaBH_4$, NaOH, and 2-mercaptoethanol (2ME).

Synthesis of Au DENs and thiol-capped Au DENs

We have previously reported the synthesis of G6-NH_2(Au_{147}) DENs.[28] Briefly, a 250 mL solution of aqueous 2.0 μM Au_{147} DENs was synthesized by adding 147 equivalents of $HAuCl_4$ to a stirred solution of 2.0 μM G6-NH_2. Au^{3+} was allowed to associate with the interior of the dendrimer for 10 min, and then a 10-fold excess of 1.0 M $NaBH_4$ in 0.30 M NaOH was added to reduce this precursor to Au_{147} DENs. The solution was stirred in air for at least 12 h to deactivate excess $NaBH_4$, and then it was divided into five 50.0 mL portions. Sufficient 2ME was added to each of these solutions to make the 2ME : Au_{147} ratio = 0, 12, 24, 50, and 72, and then the solutions were stirred for at least 5 min to ensure that the ME had sufficient time to bind to the DEN surfaces. The 2ME : Au_{147} ratios noted above were selected because previous reports have shown that Au particles in this size range are fully saturated at an alkylthiol : Au nanoparticle

ratio of 72.[29–31] DENs functionalized with 2ME are referred to as $Au_{147}@S_n$, where n is the number of surface 2ME ligands per particle, which is assumed to be equal to the amount added to solution. This assumption was tested and confirmed using Ellman's test for free thiols (ESI†).[32]

Characterization

UV-vis spectra were obtained using a Hewlett-Packard HP8453 spectrometer with a 2.00 mm path-length cuvette and a 2.0 μM G6-NH_2 solution as the blank. Scanning transmission electron microscopy (STEM) micrographs of $Au_{147}@S_0$ and $Au_{147}@S_{72}$ were obtained after EXAFS analysis (to ensure that the DENs retained their structural integrity throughout the EXAFS analysis) using a JEOL ARM 200F aberration-corrected STEM.

EXAFS analysis

The $Au_{147}@S_n$ solutions were frozen in liquid N_2 and freeze-dried in a Labconco FreeZone12 lyophilizer. For EXAFS analysis, 75–80 mg of the dried $Au_{147}@S_n$ DENs were mixed with 100 mg of BN and pressed for 30 s under 1 metric ton of pressure to form a pellet. EXAFS experiments were carried out at the National Synchrotron Light Source (Brookhaven National Laboratory) at beam line X18B. Au L3-edge data were collected at 25 ± 2 °C in transmission mode using gas ionization detector chambers. Au foil data were collected simultaneously with the sample data in reference mode.

Data were processed using the IFEFFIT software package.[33,34] The first shell fitting was done for all five datasets ($Au_{147}@S_n$, $n = 0$, 12, 24, 50, and 72) simultaneously using face-centered cubic (FCC) Au structure as the model for Au–Au bonding contributions.[35] The Au–S contributions were constructed using the coordinates of the Au_2S crystal structure. The energy correction terms and Au–S Debye–Waller factors (σ_{Au-S}^2) were not found to vary significantly with thiol concentration and were therefore constrained to be constant for all five samples. The Au–Au coordination numbers (CN_{Au-Au}), Au–Au bond lengths and disorder terms (σ_{Au-Au}^2), the Au–S bond lengths, and the Au–S coordination numbers (CN_{Au-S}) were varied independently for each of the five samples. The passive electron amplitude reduction factor was found by fitting Au foil EXAFS data prior to sample analysis and was found to be 0.84. k^2 weighting was used for all fits. The same strategy was used to fit the EXAFS signals from the MD simulations for testing of the EXAFS fitting models. For both the experimental and theoretical data, the fitting procedure used 61 independent data points to fit 25 variables.

We have considered two data analysis schemes: one that includes the third cumulant of the Au–Au bond length distribution, and the one that does not include it. We favored the second scheme, because the Au–Au and Au–S contributions overlap in the spectra, precluding accurate determination of an anharmonic correction to the Au–Au pair potential. Thus, we chose the more conservative approach, following previous reports where the effect of including the third cumulant in similar analyses was found to be very small.[17,36]

DFT-MD simulations

DFT was used to simulate the equilibrium structures of the $Au_{147}@S_n$ DENs. For each nanoparticle structure a 10 ps molecular dynamics (MD) simulation was performed at 300 K to obtain representative geometries for structural and EXAFS analysis. We used the Vienna ab initio simulation package (VASP) code[37,38] with electron correlation treated within the generalized gradient approximation using the PBEsol functional,[39] which is a modified form of Perdew–Burke–Ernzerhof (PBE) with reduced gradient dependence that improves lattice parameters and surface energies in solids. Core electrons were described with the projector augmented-wave method.[40,41] Kohn–Sham wave functions for the valence electrons were expanded in a plane wave basis set with an energy cutoff of 200 eV. The Au_{147} nanoparticle was modeled as an icosahedron structure with 20 (111) facets, and the 2ME molecule was modeled as a (–S–H) ligand to avoid the high computational cost of modeling the entire molecule. To validate the choice of SH as a model ligand, a comparison of the Au–Au PDF of $Au_{147}@(S–CH_3)_{24}$ was made with $Au_{147}@(S–H)_{24}$. The results revealed a small increase in Au–Au bond length (0.007 Å) as well as a small decrease in the disorder (-1×10^{-3} Å^2) for the $Au_{147}@(S–CH_3)_{24}$ structure. These differences are small enough to be ignored in the analysis as they would not influence any of the conclusions of this study. For all calculations, the nanoparticles were isolated in a cubic box with side lengths of 28 Å. The vacuum gap in all directions was large enough to avoid artificial interactions between periodic images.

Simulation of EXAFS from MD trajectories

Theoretical EXAFS signals were simulated using an approach similar to that reported previously.[1,2,42] The Au L3-edge EXAFS spectra were calculated from the MD trajectories by averaging the signal arising from each Au atom in the particle. Each MD simulation was allowed to thermalize for at least 4 ps and the per-configuration EXAFS spectra were calculated from snapshots of the trajectory at intervals of 20 fs for at least 4 ps giving at least 200 independent configurations in the canonical average. The 4 ps trajectory duration was found to yield converged average spectra. To ensure that 4 ps was an acceptable thermalization time, we monitored the nanoparticle structural parameters (average Au–Au bond length and bond disorder) throughout the MD trajectory. These are plotted in Fig. S1† and indicate that the particle has sufficiently thermalized. The multiple-scattering calculations were performed using FEFF6-lite.[43] All atoms up to 6.0 angstroms away from each photo-absorbing atom were included in the scattering calculations. Once the theoretical EXAFS signal was produced, the correction to the energy origin that was found for the experimental EXAFS fit was applied to the theoretical data to align the experimental and theoretical data in k-space. The Au–Au and Au–S PDFs were also produced from similarly sampled snapshots of the DFT-MD trajectories. Theoretical values for Au–Au coordination number, bond length, and bond disorder were calculated by considering all Au–Au bonding pairs between 2.5 and 3.2 Å. The selection of this window for the calculation of

theoretical coordination number, bond length, and bond disorder parameters is discussed in the next section.

Results and discussion

Nanoparticle characterization

The $Au_{147}@S_n$ DENs were characterized by UV-vis spectroscopy and electron microscopy (Fig. 1). Spectra of the thiol-capped Au DENs are similar to those in our previous report, which compared Au DENs and Au monolayer thiol-protected clusters that had been extracted from within their host dendrimers.[44] Notably, the very weak plasmon band at ~520 nm appears to be unchanged as thiols are added to the surface of the Au particles, suggesting the absence of particle agglomeration. Representative STEM micrographs for $Au_{147}@S_0$ and $Au_{147}@S_{72}$ are shown in Fig. 1, and size-distribution histograms are provided in Fig. S2.† The average particle sizes for $Au_{147}@S_0$ and $Au_{147}@S_{72}$ were 1.7 ± 0.3 nm and 1.6 ± 0.3 nm, respectively, indicating that the addition of thiol ligands does not change the DEN size.

EXAFS single-shell fitting

R-Space EXAFS spectra of $Au_{147}@S_n$ (n = 0, 12, 24, 50, and 72) are compared in Fig. 2. The results show that the first nearest neighboring Au–Au peak amplitude diminishes as n increases. As n increases, there is a clear trend showing a higher spectral amplitude in the low-Z bonding region (<2 Å) of the EXAFS spectra due to the increased Au–S bonding. Spectral contributions arising from second nearest neighbor and higher order scattering are minimal. Fig. 3 shows the EXAFS fits overlaid onto the individual spectra for $Au_{147}@S_n$.

Additionally, the individual contributions to the fits from Au–S and Au–Au paths are shown in Fig. S3.† The close agreement between the experimental data and the fit in the first nearest neighbor scattering region (R = 1.6–3.4 Å) indicates that the fit is acceptable. The region where R > 3.4 Å corresponds to additional coordination shells as well as multi-shell scattering which were not considered in the fit.

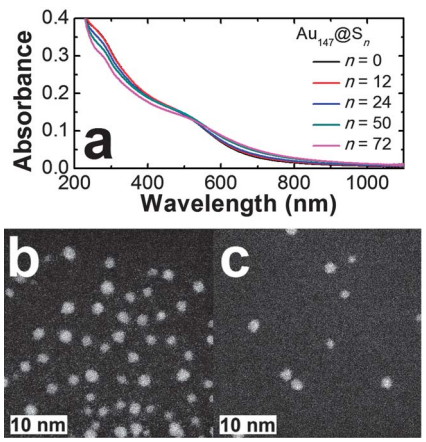

Fig. 1 (a) UV-vis spectra of $Au_{147}@S_n$ DENs (n = 0, 12, 24, 50, and 72). Representative STEM images of (b) $Au_{147}@S_0$ and (c) $Au_{147}@S_{72}$ DENs extracted from the pellet used for the EXAFS experiments following analysis. White boxes represent the 10 nm scale bar.

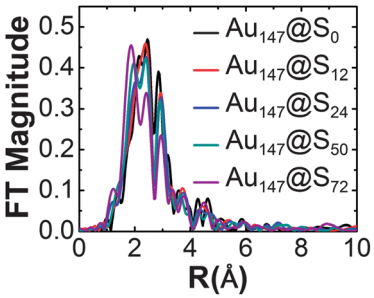

Fig. 2 A comparison of the EXAFS data in *R*-space for $Au_{147}@S_n$ DENs.

Table 1 summarizes how n affects the values of CN_{Au-S}, which were extracted from the fits. It is seen that the calculated values of CN_{Au-S} increase with the average number of thiols. The number of Au–S bonds (N_{Au-S}) per cluster was calculated according to eqn (1), where CN_{Au-S} is the number of Au–S bonds per Au atom; these results are also shown in Table 1.

$$N_{Au-S} = 147 \times CN_{Au-S} \quad (1)$$

The calculated N_{Au-S} values were then divided by the average number of thiols per particle to yield the number of Au–S bonds per surface-bound thiol ligand (N_{Au-S}/thiol, last column of Table 1). The value of N_{Au-S}/thiol provides insight into the type of binding sites occupied by the surface-confined thiols. This calculation suggests that thiols bind in 3- and 4-fold hollow sites on the Au surface at low thiol concentrations. In other words, the thiols maximize their interaction with the underlying Au surface. However, as the number of thiols per particle rises, the average number of Au–S bonds per thiol decreases until it reaches a minimum of 1.9. This observation is intuitively reasonable because it suggests that steric crowding on the surface forces the bound thiols into lower coordination sites.

The CN_{Au-Au} values for the different thiol surface coverages are plotted as a function of n in Fig. 4a (black points). The value of CN_{Au-Au} for $Au_{147}@S_0$ is 8.8 ± 0.9, which is comparable to that of a perfect 147-atom icosahedron having a CN_{Au-Au} of 8.98. The experimentally determined CN_{Au-Au} remains close to 8.98 when n = 12 and 24 but begins to decrease at higher values of n (8.0 ± 1.0 and 6.6 ± 0.9 for n = 50 and 72, respectively). This diminished coordination number is likely due to surface disorder induced by the higher surface density of thiol ligands.[1] It is also consistent with our previous findings, which showed a diminished metal–metal coordination number for Pt DENs that had electrochemically oxidized surfaces[45] as well as other reports of disordered nanoparticle systems.[3]

The average Au–Au bond lengths for each set of thiolated Au nanoparticles are plotted in Fig. 4b (black points). The value measured for $Au_{147}@S_0$ DENs was 2.811 Å ± 0.005 Å, which is consistent with a previous EXAFS report for Au nanoparticles in this size range.[46] As n increases, however, there is a slight lengthening of the average Au–Au bond length to 2.826 ± 0.005 Å at n = 50. This lengthening is likely due to the fact that thiols satisfy the under-coordinated surface Au atoms, resulting in a relaxation of the surface atoms toward an Au–Au bond length

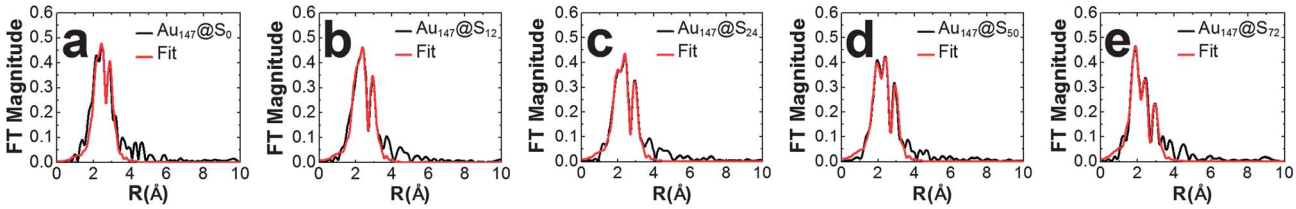

Fig. 3 *R*-Space data (black lines) and fits (red lines) for $Au_{147}@S_n$ DENs: (a) $n = 0$; (b) $n = 12$; (c) $n = 24$; (d) $n = 50$; (e) $n = 72$.

Table 1 Analysis of EXAFS fit results for Au–S bonding for $Au_{147}@S_n$ DENs

Thiols/DEN (n)	CN_{Au-S}	N_{Au-S}	N_{Au-S}/thiol
0	—	—	—
12	0.31	46	3.8
24	0.46	68	2.8
50	0.66	97	1.9
72	0.95	140	1.9

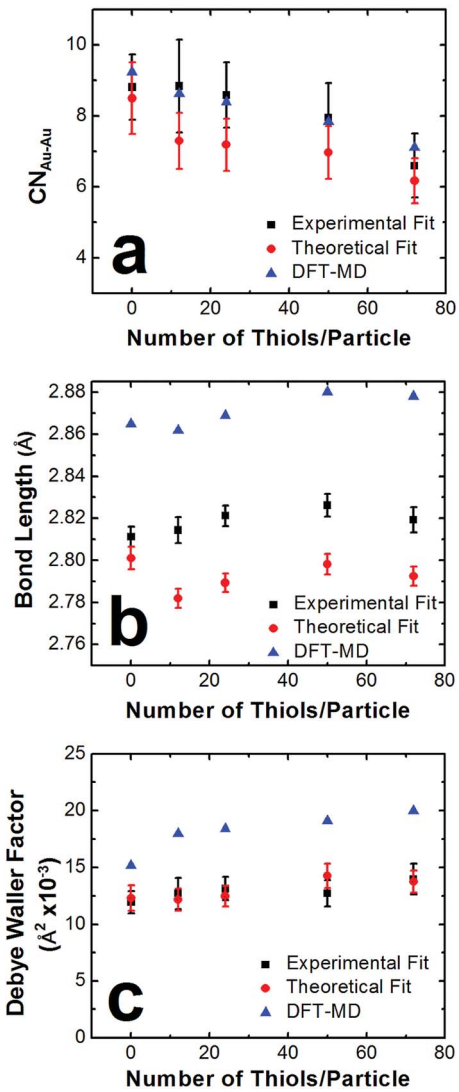

Fig. 4 Plots of structural parameters *vs.* the average number of thiols per Au DEN. (a) Au–Au coordination number; (b) Au–Au bond length; and (c) Au–Au Debye–Waller Factor.

that is closer to that in of the bulk lattice. Additionally, there are reports in the literature of thiols pulling surface atoms from smaller Au clusters to form staple motifs[47,48] which could also contribute to a longer measured average Au–Au distance.

Values of $\sigma_{Au-Au}{}^2$ that were calculated from the fits are plotted in Fig. 4c (black points). The naked Au_{147} DENs have a $\sigma_{Au-Au}{}^2$ of $11.9 \pm 1.0 \times 10^{-3}$ Å^2. As n increases, the Au–Au bond disorder also increases: 12.7 ± 1.4 ($n = 12$), 13.1 ± 1.0 ($n = 24$), 12.7 ± 1.1 ($n = 50$), and 14.0 ± 1.3 ($n = 72$). These results are consistent with increased disruption of the DEN surface driven by the thiol ligands.

Comparison of experimental and theoretical results

First-shell PDF plots for Au–Au bonding (calculated from at least 200 snapshots from the DFT-MD simulations) are shown in Fig. 5. Additionally, full Au–Au PDFs and Au–S PDFs are provided in Fig. S4 (ESI†). The first shell Au–Au PDFs were used to calculate the average Au–Au bond length, $\sigma_{Au-Au}{}^2$, and CN_{Au-Au} for $Au_{147}@S_n$ (Fig. 4, blue points). To calculate these values, a window from 2.5 to 3.2 Å was used to define the first nearest neighbor Au–Au bonds. However, because of the disorder induced by the thiol ligands, it is not possible to draw a clear distinction between the first and second nearest neighbors, and this in turn makes it difficult to precisely define average theoretical values of coordination number, bond length, and disorder. Accordingly, first shell termination values between 3.0 and 3.5 Å were considered. However, we selected a value of 3.2 Å because it is appropriate for the simulated structure of $Au_{147}@S_0$. This cutoff results in truncation of some

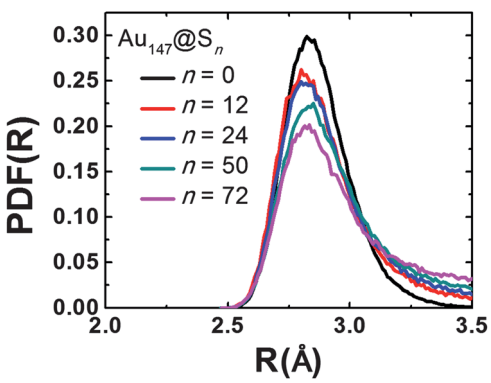

Fig. 5 First-shell Au–Au PDFs calculated using 200 independent snapshots from the DFT-MD simulations. For the calculation of the theoretical values of coordination number, bond length, and bond disorder, a window extending from $R =$ 2.5 to 3.2 Å was used.

of the longer first nearest neighbor bonds for particles having high thiol surface densities. A longer cutoff of 3.5 Å, which is more consistent with the minimum between the first and second neighbor shells in the PDF spectra, yielded poorer agreement between the theoretical parameters and the values calculated from the EXAFS fitting.

Representative images of single snapshots that were taken from the DFT-MD of $Au_{147}@S_n$ are shown in Fig. 6. Here, the thiols are displayed as thin rods to make the underlying Au structure more visible. The naked $Au_{147}@S_0$ particle appears to be icosahedral with very little distortion. However, as thiols are added to the surface of the Au_{147} core, surface disorder begins to emerge. For example, when 24 or more thiols are placed on the surface, Au–S staples are observed in the DFT-MD structure. These staples occur in the MD trajectory when the thiol surface density is sufficiently high that two thiols are bound to neighboring sites (thus sharing an Au atom). These structural motifs are discussed in more detail later. From a qualitative perspective, this is consistent with the EXAFS fitting of the experimental data, which showed increased Au–Au bond length and σ_{Au-Au}^2 as thiols were added.

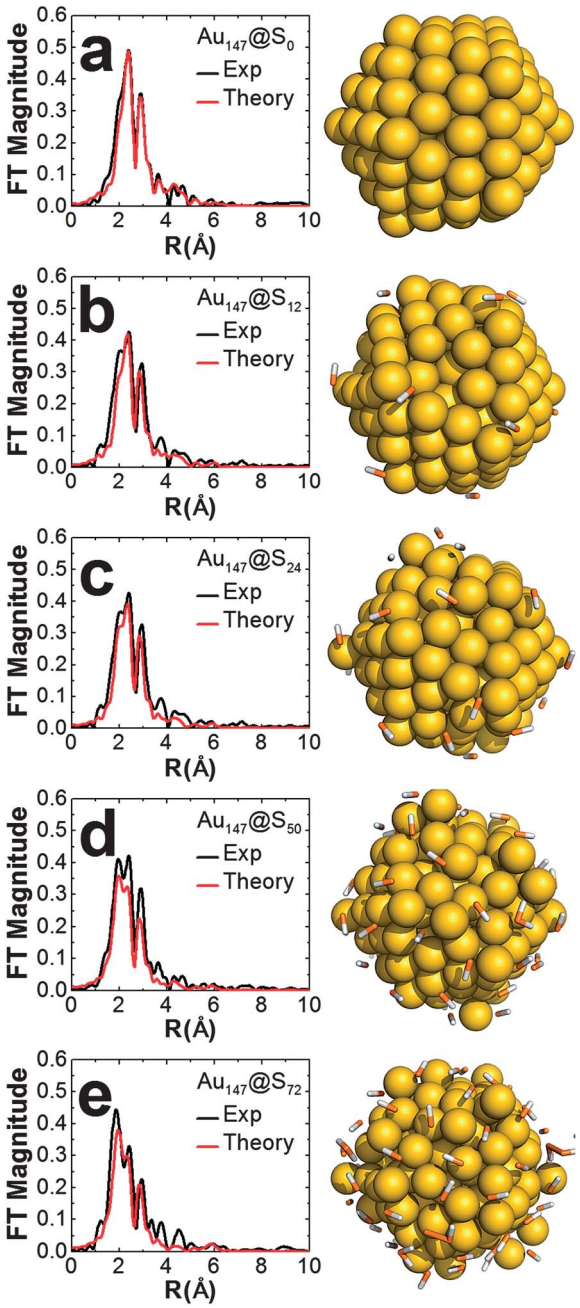

Fig. 6 Left side. Comparison of experimentally and theoretically derived EXAFS data in *R*-space: (a) $Au_{147}@S_0$, (b) $Au_{147}@S_{12}$, (c) $Au_{147}@S_{24}$, (d) $Au_{147}@S_{50}$, (e) $Au_{147}@S_{72}$. Right side: Representative snapshots of the DFT-MD trajectories taken from the portion of the simulations used to calculate the theoretical EXAFS signals and PDFs.

Comparisons of the experimentally and theoretically derived EXAFS data in *R*-space are plotted in Fig. 6. There is good agreement in every case. Additionally, comparisons of the real and imaginary parts of the experimental and theoretical Fourier transforms are shown for $Au_{147}@S_0$ in Fig. S6.† Importantly, this validation of the DFT-MD simulations *via* the consistency between the experimental and theoretical EXAFS signals allows us to draw two conclusions. First, the DFT-MD simulations accurately model the Au structure. Second, the theoretical EXAFS spectra are generated correctly from the configuration and time averaging of the FEFF scattering calculations.

The theoretical EXAFS signals were fit using the same parameters as for the previously discussed experimental data, and the results for CN_{Au-Au}, Au–Au bond length, and σ_{Au-Au}^2 are plotted in Fig. 4 (red points). The trend in CN_{Au-Au} as a function of the surface thiol density is similar to that observed for the experimental data (Fig. 4a). The average CN_{Au-Au} decreases from 8.5 to 6.3 as the simulated particles go from uncapped to saturated with thiols. The values for CN_{Au-Au} plotted in Fig. 4a are within the errors of the experimental data, but, in general, are slightly lower than the values extracted from the DFT-MD-derived PDFs.

Fig. 4b summarizes the bond lengths calculated from the experimental and theoretical EXAFS fits, as well as the values taken directly from the DFT-MD simulations. According to the DFT-MD simulations, the Au–Au bonds lengthen slightly as thiols are added to the surface, and this trend is also observed for the experimental data. However, the magnitudes of the bond lengths derived from the experimental data are significantly shorter than those calculated from the simulation PDFs. Likewise, the EXAFS fits of the theoretical data do not agree with the DFT-MD simulations. Specifically, fit values of the theoretical EXAFS signals for bond length are slightly shorter than the experimental fit results, but this discrepancy is within the systematic uncertainty for DFT calculations of bond length (~1%).[39]

Fig. 4c summarizes the values of σ_{Au-Au}^2 for the experimental and theoretical data fits and for the DFT-MD simulations. This plot indicates that the fitting underestimates σ_{Au-Au}^2 as compared to the DFT-MD values, but excellent agreement is observed between the fits of the experimental and theoretical EXAFS spectra. The underestimation of disorder and bond length in the fits, as compared to the calculated values from the DFT-MD simulations, indicates that the EXAFS fitting is not accounting for the longest Au–Au bonds observed in the DFT-MD derived structures. This is likely due to the Gaussian bond length distribution approximation that is assumed when fitting

EXAFS. This self-consistency check of comparing structural parameters calculated directly from the DFT-MD simulations to the fit of calculated EXAFS spectra for such particles is further proof that the standard fitting model is not able to describe highly disordered nanoparticles.

To further understand the observed differences between the theoretical and experimental values of the CN_{Au-Au}, bond length, and σ_{Au-Au}^2, Gaussian curves describing the first shell Au–Au bonding were plotted for each of the experimental samples. The parameters for the Gaussians (average bond lengths, standard deviations, and areas under the curves) were taken directly from the values calculated from the EXAFS fits of the experimental data (Fig. 7, red lines). These were plotted on the same scale as the first shell Au–Au PDFs generated from the equilibrated structures of the DFT-MD simulations (Fig. 7, black lines).

This comparison demonstrates the segment of the first shell Au–Au bonds that are described in the EXAFS fits by the Gaussian approximation. The shortest Au–Au bond lengths ($R < \sim 3.0$ Å) derived from the PDFs are well described by the Gaussians. Likewise, the peak positions of the Gaussians and PDFs are also in good agreement, but the heights of the Gaussians are generally slightly higher than the first nearest neighbor PDFs determined from the DFT-MD simulations. Importantly, the assumption that the bond lengths are distributed as a Gaussian fails at $R > 3.0$ Å. This observation helps to rationalize the differences that are observed between the experimental and DFT-MD results. Because the Gaussians taken from the EXAFS fits underestimate the number of long Au–Au bonds (>3.0 Å), the values of the average Au–Au bond length and σ_{Au-Au}^2 that are calculated from the fits are also underestimated. This is observed in the black and red points in Fig. 4b and c which are low in relation to the blue (theoretical) points. Conversely, the experimental results for CN_{Au-Au} are very close to the theoretical values. This is because while the longer Au–Au bonds in the first shells are missed, the EXAFS fit Gaussians are higher in amplitude (describing additional shorter bonds).

As mentioned earlier, no higher order terms in the cumulant expansion were used to fit the datasets due to the overlapping Au–S and Au–Au bonding contributions. From the comparisons of the Gaussians generated from the experimental EXAFS data and the Au–Au PDFs calculated from theory, one could imagine that fitting the Au–Au scattering paths with third cumulants would lead to closer correspondence by accounting for the asymmetry of the Gaussians.[3] However, to reduce fitting artifacts arising from the overlapping Au–S and Au–Au bonding contributions, the use of a cumulant expansion was not investigated in this work. The EXAFS analysis outlined here is well suited for probing this issue and is a topic of ongoing work in our labs.

Au–S interfacial structure

Previous reports of Au nanoparticles having thiolated shells have established the presence of structural motifs called staples,[23,25,48–50] and these features must also be considered here. Here, staples are defined as a Au atom displaced from the surface of the DEN structure by bound thiols. The DFT-MD simulations show that when two thiols share a single surface Au atom, that atom is lifted out of the Au lattice. This is clearly observed in the nanoparticle image snapshots of $Au_{147}@S_{24}$, $Au_{147}@S_{50}$, and $Au_{147}@S_{72}$ (Fig. 6c–e, respectively). These surface staples are slightly different from the stellated Au staple structures reported for Au_{25} nanoclusters,[23,49,51] but similar to the monomeric Au staples observed in larger (Au_{38}) nanoclusters.[25] They are also consistent with the increased disorder observed at high thiol concentrations (Fig. 4c) and the decrease in CN_{Au-Au} (Fig. 4a).

We carried out an analysis of the experimental Au–S bond length data in an effort to detect Au atoms pulled out of the nanoparticle surface by the thiols. As discussed earlier and demonstrated by the DFT-MD results, we anticipate a higher probability of observing staple structures at high thiol coverages. This is because staples are strongly correlated to motifs wherein two thiols share a single Au surface atom, and the probability of this happening increases with thiol surface concentration. Staples are characterized by a decrease in Au–Au interactions and an increase in Au–S interactions, and therefore stapled Au atoms have shorter Au–S bond lengths compared to a thiol bound to a gold atom in an extended lattice. For example, Heaven *et al.*[23] and Qian *et al.*[25] determined the crystal structure of $Au_{25}@S_{18}$ and $Au_{38}@S_{24}$ nanoclusters, respectively, and observed surface staple motifs. Both reports showed that S atoms bound to Au atoms within the central Au nanocluster have a bond length of approximately 2.38 Å, while the stellated S–Au–S structures have a Au–S bond length of 2.30 to 2.32 Å.

The average Au–S bond lengths calculated from the EXAFS fits of the experimental data for the $Au_{147}@S_n$ DENs are 2.349 ± 0.031 Å ($n = 12$), 2.326 ± 0.014 Å ($n = 24$), 2.318 ± 0.011 Å ($n = 50$), and 2.295 ± 0.006 Å ($n = 72$). This decreasing trend in the length of the Au–S bonds is fully consistent with both literature reports[23,25] and DFT-MD data (Fig. S4b†) and suggests the presence of surface staples.

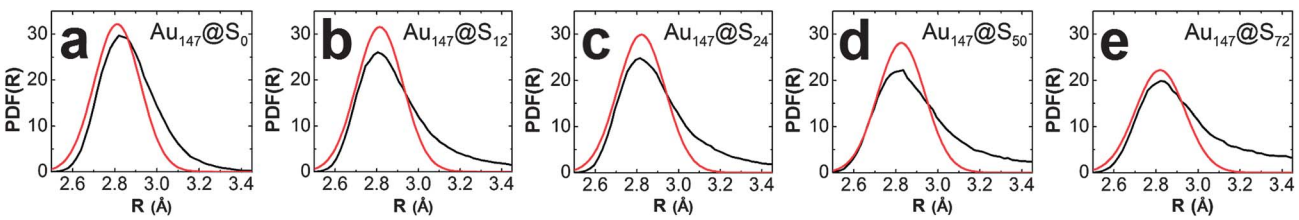

Fig. 7 First nearest neighbor Au–Au PDFs taken from the DFT-MD structures (black lines) with the EXAFS Gaussian approximations from experimental data fits overlaid (red lines) for $Au_{147}@S_n$. (a) $n = 0$, (b) 12, (c) 24, (d) 50, and (e) 72.

Summary and conclusions

Here we showed that a combined experimental/theoretical approach for interpreting EXAFS data leads to more detailed information about the structure of nanoparticles than standard EXAFS fitting techniques. This comparison was enabled by the experimental DEN model, which provides a simple system for progressively introducing structural disorder *via* interactions with different surface concentrations of ligands.

There are a number of important outcomes of this study. First, the DFT-MD simulations reported here accurately depict complex experimental systems in which control is exerted over the disorder of Au_{147} DENs. This point was verified by the validation of the DFT-MD nanoparticle structures by comparing theoretically derived EXAFS signals with experimental signals on analogous particle systems. Second, the shortcomings of the Gaussian bond length disorder approximation was probed, showing that standard EXAFS fitting models do not accurately describe strongly and asymmetrically disordered systems. We were able to demonstrate this by directly comparing theoretical DFT-MD derived from PDFs with Gaussian functions describing the first-shell Au–Au interactions taken from experimental EXAFS fits. Third, a more detailed understanding of the Au–S interface for thiol-capped Au nanoparticles was achieved by combining both experimental and theoretical results.

Acknowledgements

We gratefully acknowledge support from the Chemical Sciences, Geosciences, and Biosciences Division, Office of Basic Energy Sciences, Office of Science, U. S. Department of Energy (Contract: DE-FG02-09ER16090). RMC thanks the Robert A. Welch Foundation (Grant F-0032) for sustained support. The computational work was done primarily at the National Energy Research Scientific Computing Center and the Texas Advanced Computing Center. AIF acknowledges support of the Department of Energy Grant no. DE-FG02-03ER15476. Use of the NSLS is supported by the U.S. Department of Energy, Office of Science, Office of Basic Energy Sciences, under Contract no. DE-AC02-98CH10886. Beamline X18B at the NSLS is supported in part by the Synchrotron Catalysis Consortium, U. S. Department of Energy Grant no. DE-FG02-05ER15688. The electron microscope used for this project was supported by a grant from the National Institute on Minority Health and Health Disparities (G12MD007591) from the National Institutes of Health. DFY would like to thank Rachel M. Anderson for help with EXAFS data collection and many helpful discussions and Daniel Bahena for assistance with collecting STEM images.

References

1 A. Yevick and A. I. Frenkel, Effects of surface disorder on EXAFS modeling of metallic clusters, *Phys. Rev. B: Condens. Matter Mater. Phys.*, 2010, **81**, 115451.

2 O. M. Roscioni, N. Zonias, S. W. T. Price, A. E. Russell, T. Comaschi and C.-K. Skylaris, Computational prediction of L3 EXAFS spectra of gold nanoparticles from classical molecular dynamics simulations, *Phys. Rev. B: Condens. Matter Mater. Phys.*, 2011, **83**, 115409.

3 S. W. T. Price, N. Zonias, C.-K. Skylaris, T. I. Hyde, B. Ravel and A. E. Russell, Fitting EXAFS data using molecular dynamics outputs and a histogram approach, *Phys. Rev. B: Condens. Matter Mater. Phys.*, 2012, **85**, 075439.

4 A. I. Frenkel, A. Yevick, C. Cooper and R. Vasic, Modeling the Structure and Composition of Nanoparticles by Extended X-Ray Absorption Fine-Structure Spectroscopy, *Annu. Rev. Anal. Chem.*, 2011, **4**, 23.

5 A. I. Frenkel, Applications of extended X-ray absorption fine-structure spectroscopy to studies of bimetallic nanoparticle catalysts, *Chem. Soc. Rev.*, 2012, **41**, 8163.

6 A. I. Frenkel, Q. Wang, S. I. Sanchez, M. W. Small and R. G. Nuzzo, *J. Chem. Phys.*, 2013, **138**, 064202.

7 E. A. Stern and S. M. Heald, Basic Principles and Applications of EXAFS, in *Handbook of Synchrotron Radiation*, ed. E. E. Koch, North-Holland, 1983, pp. 995–1014.

8 F. Vila, J. J. Rehr, J. Kas, R. G. Nuzzo and A. I. Frenkel, Dynamic structure in supported Pt nanoclusters: Real-time density functional theory and X-ray spectroscopy simulations, *Phys. Rev. B: Condens. Matter Mater. Phys.*, 2008, **78**, 121404.

9 V. S. Myers, M. G. Weir, E. V. Carino, D. F. Yancey, S. Pande and R. M. Crooks, Dendrimer-encapsulated nanoparticles: New synthetic and characterization methods and catalytic applications, *Chem. Sci.*, 2011, **2**, 1632.

10 S. I. Sanchez, L. D. Menard, A. Bram, J. H. Kang, M. W. Small, R. G. Nuzzo and A. I. Frenkel, The Emergence of Nonbulk Properties in Supported Metal Clusters: Negative Thermal Expansion and Atomic Disorder in Pt Nanoclusters Supported on γ-Al_2O_3, *J. Am. Chem. Soc.*, 2009, **131**, 7040.

11 M. W. Small, S. I. Sanchez, N. S. Marinkovic, A. I. Frenkel and R. G. Nuzzo, Influence of Adsorbates on the Electronic Structure, Bond Strain, and Thermal Properties of an Alumina-Supported Pt Catalyst, *ACS Nano*, 2012, **6**, 5583.

12 S. Mostafa, F. Behafarid, J. R. Croy, L. K. Ono, L. Li, J. C. Yang, A. I. Frenkel and B. R. Cuenya, Shape-Dependent Catalytic Properties of Pt Nanoparticles, *J. Am. Chem. Soc.*, 2010, **132**, 15714.

13 B. Roldan Cuenya, J. R. Croy, S. Mostafa, F. Behafarid, L. Li, Z. Zhang, J. C. Yang, Q. Wang and A. I. Frenkel, Solving the Structure of Size-Selected Pt Nanocatalysts Synthesized by Inverse Micelle Encapsulation, *J. Am. Chem. Soc.*, 2010, **132**, 8747.

14 O. M. Wilson, R. W. J. Scott, J. C. Garcia-Martinez and R. M. Crooks, Separation of Dendrimer-Encapsulated Au and Ag Nanoparticles by Selective Extraction, *Chem. Mater.*, 2004, **16**, 4202.

15 O. M. Wilson, R. W. J. Scott, J. C. Garcia-Martinez and R. M. Crooks, Synthesis, Characterization, and Structure-Selective Extraction of 1–3 nm Diameter AuAg Dendrimer-Encapsulated Bimetallic Nanoparticles, *J. Am. Chem. Soc.*, 2005, **127**, 1015.

16 R. Sardar, A. M. Funston, P. Mulvaney and R. W. Murray, Gold Nanoparticles: Past, Present, and Future, *Langmuir*, 2009, **25**, 13840.

17 A. I. Frenkel, S. Nemzer, I. Pister, L. Soussan, T. Harris, Y. Sun and M. H. Rafailovich, Size-controlled synthesis and characterization of thiol-stabilized gold nanoparticles, *J. Chem. Phys.*, 2005, **123**, 184701.

18 C. López-Cartes, T. C. Rojas, R. Litrán, D. Martínez-Martínez, J. M. de la Fuente, S. Penadés and A. Fernández, Gold Nanoparticles with Different Capping Systems: An Electronic and Structural XAS Analysis, *J. Phys. Chem. B*, 2005, **109**, 8761.

19 J. M. Ramallo-López, L. J. Giovanetti, F. G. Requejo, S. R. Isaacs, Y. S. Shon and M. Salmeron, Molecular conformation changes in alkylthiol ligands as a function of size in gold nanoparticles: X-ray absorption studies, *Phys. Rev. B: Condens. Matter Mater. Phys.*, 2006, **74**, 073410.

20 Y. Sun, A. I. Frenkel, H. White, L. Zhang, Y. Zhu, H. Xu, J. C. Yang, T. Koga, V. Zaitsev, M. H. Rafailovich and J. C. Sokolov, Comparison of Decanethiolate Gold Nanoparticles Synthesized by One-Phase and Two-Phase Methods, *J. Phys. Chem. B*, 2006, **110**, 23022.

21 P. Zhang, A. Y.-C. Chu, T.-K. Sham, Y. Yao and S.-T. Lee, Chemical synthesis and structural studies of thiol-capped gold nanoparticles, *Can. J. Chem.*, 2009, **87**, 335.

22 M. M. Mariscal, J. A. Olmos-Asar, C. Gutierrez-Wing, A. Mayoral and M. J. Yacaman, On the atomic structure of thiol-protected gold nanoparticles: a combined experimental and theoretical study, *Phys. Chem. Chem. Phys.*, 2010, **12**, 11785.

23 M. W. Heaven, A. Dass, P. S. White, K. M. Holt and R. W. Murray, Crystal Structure of the Gold Nanoparticle $[N(C_8H_{17})_4][Au_{25}(SCH_2CH_2Ph)_{18}]$, *J. Am. Chem. Soc.*, 2008, **130**, 3754.

24 M. Zhu, C. M. Aikens, F. J. Hollander, G. C. Schatz and R. Jin, Correlating the Crystal Structure of A Thiol-Protected Au_{25} Cluster and Optical Properties, *J. Am. Chem. Soc.*, 2008, **130**, 5883.

25 H. Qian, W. T. Eckenhoff, Y. Zhu, T. Pintauer and R. Jin, Total Structure Determination of Thiolate-Protected Au_{38} Nanoparticles, *J. Am. Chem. Soc.*, 2010, **132**, 8280.

26 P. D. Jadzinsky, G. Calero, C. J. Ackerson, D. A. Bushnell and R. D. Kornberg, Structure of a Thiol Monolayer-Protected Gold Nanoparticle at 1.1 Å Resolution, *Science*, 2007, **318**, 430.

27 E. Torres, A. T. Blumenau and P. U. Biedermann, Steric and Chain Length Effects in the (sqrt(3) × sqrt(3))R30° Structures of Alkanethiol Self-Assembled Monolayers on Au(111), *ChemPhysChem*, 2011, **12**, 999.

28 D. F. Yancey, L. Zhang, R. M. Crooks and G. Henkelman, Au@Pt dendrimer encapsulated nanoparticles as model electrocatalysts for comparison of experiment and theory, *Chem. Sci.*, 2012, **3**, 1033.

29 O. Lopez-Acevedo, J. Akola, R. L. Whetten, H. Grönbeck and H. Häkkinen, Structure and Bonding in the Ubiquitous Icosahedral Metallic Gold Cluster $Au_{144}(SR)_{60}$, *J. Phys. Chem. C*, 2009, **113**, 5035.

30 E. Heikkilä, A. A. Gurtovenko, H. Martinez-Seara, H. Häkkinen, I. Vattulainen and J. Akola, Atomistic Simulations of Functional $Au_{144}(SR)_{60}$ Gold Nanoparticles in Aqueous Environment, *J. Phys. Chem. C*, 2012, **116**, 9805.

31 J.-P. Choi and R. W. Murray, Electron Self-Exchange Between $Au_{140}^{+/0}$ Nanoparticles Is Faster Than That Between $Au_{38}^{+/0}$ in Solid-State, Mixed-Valent Films, *J. Am. Chem. Soc.*, 2006, **128**, 10496.

32 J. Sedlak and R. H. Lindsay, Estimation of total, protein-bound, and nonprotein sulfhydryl groups in tissue with Ellman's reagent, *Anal. Biochem.*, 1968, **25**, 192.

33 M. Newville, IFEFFIT: interactive XAFS analysis and FEFF fitting, *J. Synchrotron Radiat.*, 2001, **8**, 322.

34 B. Ravel and M. Newville, ATHENA, ARTEMIS, HEPHAESTUS: data analysis for X-ray absorption spectroscopy using IFEFFIT, *J. Synchrotron Radiat.*, 2005, **12**, 537.

35 V. Petkov, N. Bedford, M. R. Knecht, M. G. Weir, R. M. Crooks, W. Tang, G. Henkelman and A. Frenkel, Periodicity and Atomic Ordering in Nanosized Particles of Crystals, *J. Phys. Chem. C*, 2008, **112**, 8907.

36 L. D. Menard, H. Xu, S.-P. Gao, R. D. Twesten, A. S. Harper, Y. Song, G. Wang, A. D. Douglas, J. C. Yang, A. I. Frenkel, R. W. Murray and R. G. Nuzzo, Metal Core Bonding Motifs of Monodisperse Icosahedral Au_{13} and Larger Au Monolayer-Protected Clusters As Revealed by X-ray Absorption Spectroscopy and Transmission Electron Microscopy, *J. Phys. Chem. B*, 2006, **110**, 14564.

37 G. Kresse, Dissociation and sticking of H_2 on the Ni(111), (100), and (110) substrate, *Phys. Rev. B: Condens. Matter Mater. Phys.*, 2000, **62**, 8295.

38 G. Kresse and J. Hafner, First-principles study of the adsorption of atomic H on Ni (111), (100) and (110), *Surf. Sci.*, 2000, **459**, 287.

39 J. P. Perdew, A. Ruzsinszky, G. I. Csonka, O. A. Vydrov, G. E. Scuseria, L. A. Constantin, X. Zhou and K. Burke, Restoring the Density-Gradient Expansion for Exchange in Solids and Surfaces, *Phys. Rev. Lett.*, 2008, **100**, 136406.

40 P. E. Blochl, Projector augmented-wave method, *Phys. Rev. B: Condens. Matter Mater. Phys.*, 1994, **50**, 17953.

41 G. Kresse and D. Joubert, From ultrasoft pseudopotentials to the projector augmented-wave method, *Phys. Rev. B: Condens. Matter Mater. Phys.*, 1999, **59**, 1758.

42 M. A. MacDonald, P. Zhang, N. Chen, H. Qian and R. Jin, Solution-Phase Structure and Bonding of $Au_{38}(SR)_{24}$ Nanoclusters from X-ray Absorption Spectroscopy, *J. Phys. Chem. C*, 2011, **115**, 65.

43 S. I. Zabinsky, J. J. Rehr, A. Ankudinov, R. C. Albers and M. J. Eller, Multiple-scattering calculations of X-ray-absorption spectra, *Phys. Rev. B: Condens. Matter Mater. Phys.*, 1995, **52**, 2995.

44 Y.-G. Kim, J. C. Garcia-Martinez and R. M. Crooks, Electrochemical Properties of Monolayer-Protected Au and Pd Nanoparticles Extracted from with Dendrimer Templates, *Langmuir*, 2005, **21**, 5485.

45 V. S. Myers, A. I. Frenkel and R. M. Crooks, *In situ* Structural Characterization of Platinum Dendrimer-Encapsulated Oxygen Reduction Electrocatalysts, *Langmuir*, 2012, **28**, 1596.

46 J. T. Miller, A. J. Kropf, Y. Zha, J. R. Regalbuto, L. Delannoy, C. Louis, E. Bus and J. A. van Bokhoven, The effect of gold

particle size on AuAu bond length and reactivity toward oxygen in supported catalysts, *J. Catal.*, 2006, **240**, 222.

47 M. A. MacDonald, P. Zhang, H. Qian and R. Jin, Site-Specific and Size-Dependent Bonding of Compositionally Precise Gold–Thiolate Nanoparticles from X-ray Spectroscopy, *J. Phys. Chem. Lett.*, 2010, **1**, 1821.

48 G. A. Simms, J. D. Padmos and P. Zhang, Structural and electronic properties of protein/thiolate-protected gold nanocluster with "staple" motif: A XAS, L-DOS, and XPS study, *J. Chem. Phys.*, 2009, **131**, 214703.

49 M. A. MacDonald, D. M. Chevrier, P. Zhang, H. Qian and R. Jin, The Structure and Bonding of $Au_{25}(SR)_{18}$ Nanoclusters from EXAFS: The Interplay of Metallic and Molecular Behavior, *J. Phys. Chem. C*, 2011, **115**, 15282.

50 Y. Pei, Y. Gao, N. Shao and X. C. Zeng, Thiolate-Protected $Au_{20}(SR)_{16}$ Cluster: Prolate Au_8 Core with New $[Au_3(SR)_4]$ Staple Motif, *J. Am. Chem. Soc.*, 2009, **131**, 13619.

51 W. Kurashige, M. Yamaguchi, K. Nobusada and Y. Negishi, Ligand-Induced Stability of Gold Nanoclusters: Thiolate *versus* Selenolate, *J. Phys. Chem. Lett.*, 2012, **3**, 2649.